KLK6 expression in skin induces PAR1-mediated psoriasiform dermatitis and inflammatory joint disease

Allison C. Billi[1†], Jessica E. Ludwig[2,3†], Yi Fritz[2†], Richard Rozic[4], William R. Swindell[1,5,6], Lam C. Tsoi[1,7,8], Dennis Gruzska[2,3], Shahla Abdollahi-Roodsaz[9], Xianying Xing[1], Doina Diaconu[2], Ranjitha Uppala[1], Maya I. Camhi[2], Philip A. Klenotic[2], Mrinal K. Sarkar[1], M. Elaine Husni[10], Jose U. Scher[11], Christine McDonald[12], J. Michelle Kahlenberg[13], Ronald J. Midura[4], Johann E. Gudjonsson[1], and Nicole L. Ward[2,3,14*] ORCID ID 0000-0003-1907-2621

[1]Department of Dermatology, University of Michigan, Ann Arbor, MI, USA
[2]Department of Dermatology, Case Western Reserve University, Cleveland, OH, USA
[3]Department of Nutrition, Case Western Reserve University, Cleveland, OH, USA
[4]Department of Biomedical Engineering, Lerner Research Institute, Cleveland Clinic, Cleveland, OH, USA
[5]Ohio University, Heritage College of Osteopathic Medicine, Athens, OH, USA
[6]The Jewish Hospital, Department of Internal Medicine, Cincinnati, OH, USA
[7]Department of Biostatistics, Center for Statistical Genetics, University of Michigan, Ann Arbor, MI, USA
[8]Department of Computational Medicine and Bioinformatics, University of Michigan, Ann Arbor, MI, USA
[9]Inflammation and Immunology Thematic Center of Excellence, Celgene Corp., Cambridge, MA, USA
[10]Department of Rheumatologic and Immunologic Disease, Cleveland Clinic, Cleveland, OH, USA
[11]Department of Medicine, New York University, New York, NY, USA
[12]Department of Inflammation and Immunity, Lerner Research Institute, Cleveland Clinic, Cleveland, OH, USA
[13]Department of Internal Medicine, University of Michigan, Ann Arbor, MI, USA
[14]Murdough Family Center for Psoriasis, Cleveland, OH, USA

[†] These authors share the first author position.

[*]Address for correspondence:
Dr. Nicole L. Ward
Case Western Reserve University
10900 Euclid Ave,
Cleveland, OH 44106
nlw4@cwru.edu

Conflict of interest statement: The authors have declared that no conflict of interest exists.

Supplemental figure titles and legends

A

Symbol	Log_2 FC in *Klk6*+ mice
Il22	10.125
Mug2	9.901
Prl2c5	9.857
Prl2c2	9.745
Mug1	9.539
Gm5416	9.406
Klk6	9.388
Sprr2e	9.243
Il17a	9.177
Sprr2f	9.086
Ankk1	9.042
Sprr2i	9.041
Uox	9.023
Sprr2d	8.995
Defb3	8.96
Sprr2b	8.955
Lce3b	8.941
Sprr2k	8.916
Lce3a	8.889
Sprr1b	8.782
BC117090	8.769
Sprr2h	8.767
S100a9	8.693
Stfa3	8.641
S100a8	8.617
Stfa1	8.605
BC100530	8.602
Il17f	8.562
Il19	8.54
Serpinb3a	8.532
Lce3f	8.52
Prl2c1	8.512
Lce3d	8.463
Pla2g4d	8.461
Lce3e	8.442
Cdhr1	8.397
Iltifb	8.371
Stfa2	8.245
Cxcl3	8.221
Slc26a4	8.209
Nppb	8.206
Il24	8.19
Gm5483	8.132
Saa3	8.074
Chil1	7.905
Lcn2	7.866
Saa2	7.839
Prl2c3	7.835
Prl2a1	7.826
Spdef	7.787

B

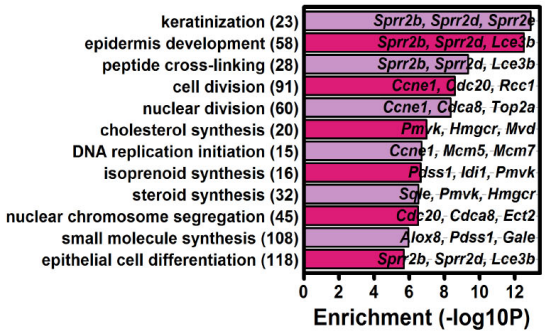

C

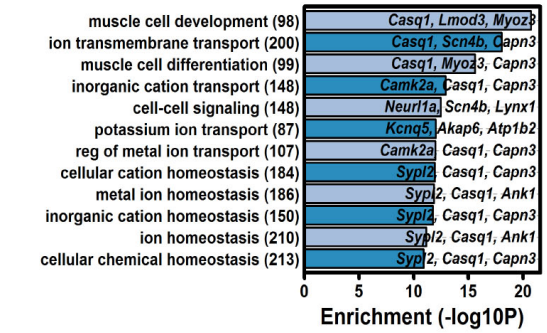

D

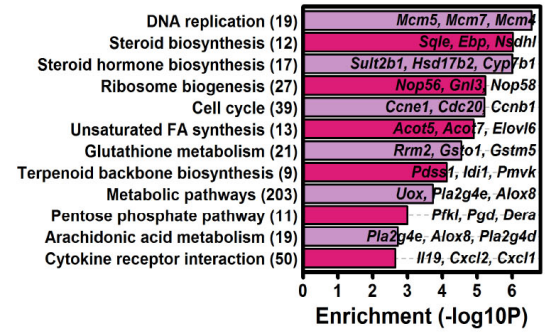

E

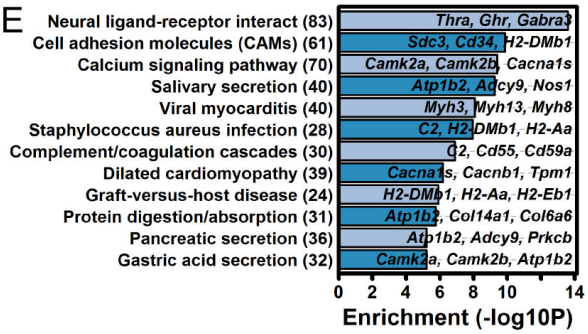

Figure S1. Top-ranking Gene Ontology (GO) and KEGG terms associated with differentially enriched genes (DEGs) identified in *Klk6*+ *vs* control dorsal skin.
(A) List of the 50 top *Klk6*+-increased DEGs by fold change (FC). See **Table S2** for full list of DEGs.
(B) GO biological process terms associated with *Klk6*+-increased DEGs (false discovery rate (FDR)<0.10, FC>2.0).
(C) GO biological process terms associated with *Klk6*+-decreased DEGs (FDR<0.10, FC<0.50).
(D) KEGG terms associated with *Klk6*+-increased DEGs (FDR<0.10, FC>2.0).
(E) KEGG terms associated with *Klk6*+-decreased DEGs (FDR<0.10, FC<0.50).

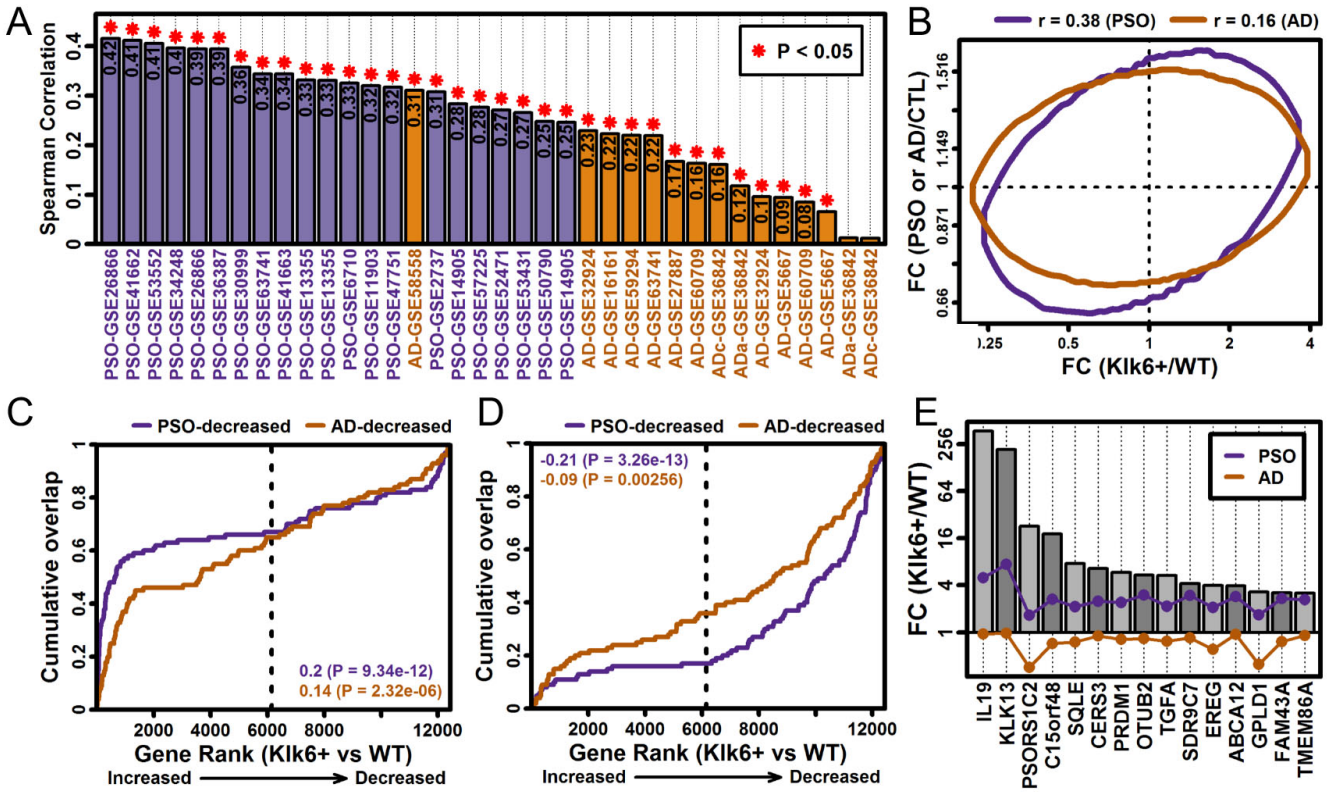

Figure S2. The *Klk6*+ lesional skin transcriptome corresponds better to the lesional skin expression profile of psoriasis (PSO) than atopic dermatitis (AD).
(A) Spearman correlations. FC estimates (*Klk6*+/WT) were compared to those obtained from 36 comparisons yielding PSO/CTL (*n* = 21) or AD/CTL (*n* = 15) FC estimates (ADa = acute atopic dermatitis; ADc = chronic atopic dermatitis). The 36 comparisons are ranked based upon the Spearman correlation coefficient estimate.
(B) Correlation between *Klk6*+/WT FC estimates and average FC estimates from PSO (*n* = 11) and AD (*n* = 10) (Affymetrix Human Genome Plus 2.0 array platform only). Ellipses outline the middle 75% of genes closest to the bivariate median based upon the Mahalanobis distance (top margin: Spearman correlations).
(C) Gene set enrichment analysis (GSEA) of PSO/AD-increased genes.
(D) GSEA of PSO/AD-decreased genes. In **C** and **D**, the top 100 genes most strongly increased or decreased in each disease were analyzed. The figure shows cumulative overlap of these genes (vertical axis) with genes ranked based upon *Klk6*+/WT FC estimates (horizontal axis). The area between each curve and the diagonal is shown with corresponding P values (Wilcoxon rank sum test). For the 100 genes most strongly elevated in each human disease, overlap with genes increased in *Klk6*+ transgenic skin is stronger for PSO-increased genes ($P=9.3x10^{-12}$) than AD-increased genes ($P = 2.3x10^{-6}$); similarly, overlap with genes decreased in *Klk6*+ transgenic skin is stronger for PSO-decreased genes ($P = 3.13x10^{-13}$) than AD-increased genes (P = 0.00256).
(E) Example genes increased in *Klk6*+ mouse and PSO lesions but not AD lesions.

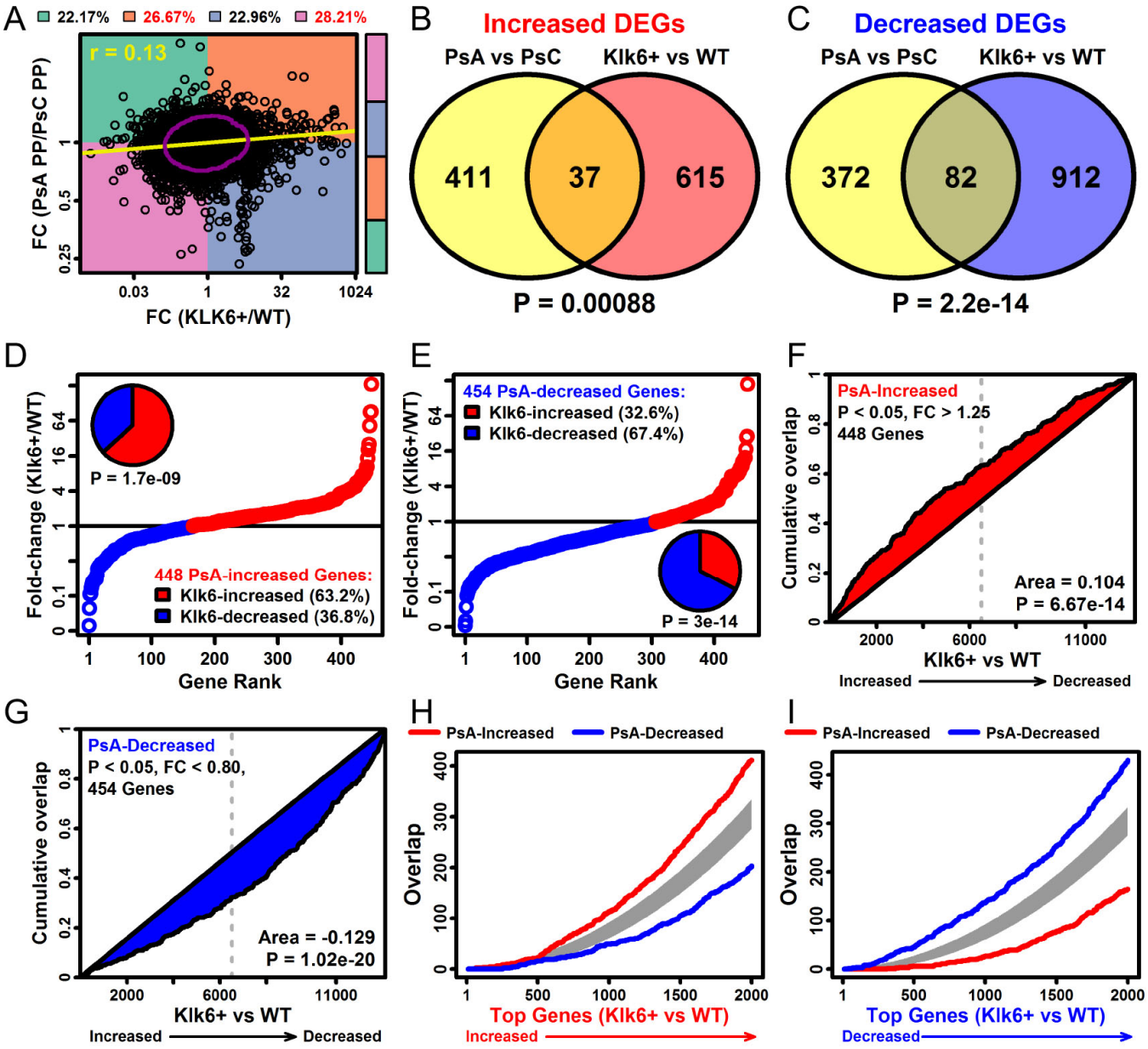

Figure S3. Genes with altered expression in *Klk6+* transgenic skin overlap significantly with those altered in psoriatic arthritis (PsA) vs cutaneous-only psoriasis (PsC) lesional skin.
(A) Scatterplot depicting fold change (FC) estimates for 13137 human-mouse gene pairs with identical gene symbols derived from comparisons of *Klk6+* vs WT control dorsal skin and PsA vs PsC lesional skin. Percentage of genes in each quadrant is indicated, with red font indicating P<0.05 by Fisher's exact test. Yellow line, robust regression estimate; upper left, Spearman rank correlation; ellipse, 90% of genes nearest to bivariate mean, Mahalanobis distance.
(B) Venn diagram showing overlap and P value by Fisher's exact test for overlap of differentially enriched genes (DEGs) increased in PsA vs PsC and *Klk6+* vs WT skin. PsA-altered genes are defined as P<0.05 with FC>1.25 or FC<0.80.
(C) Venn diagram showing overlap and P value of decreased DEGs.
(D) FC estimates for DEGs increased in PsA. Pie chart represents the portion of genes increased (red) and decreased (blue) in *Klk6+*.
(E) FC estimates for DEGs decreased in PsA. Pie chart represents the portion of genes increased (red) and decreased (blue) in *Klk6+*.
(F,G) Gene set enrichment analysis (GSEA) showing cumulative overlap between PsA-increased (**F**) or PsA-decreased (**G**) genes (vertical axis) and a gene list ranked based on decreasing expression in *Klk6+* vs WT (horizontal axis).
(H,I) Non-cumulative overlap between PsA-increased (**H**) or PsA-decreased (**I**) genes and a gene list ranked based on increasing expression in *Klk6+* vs WT. Overlap beyond the gray region is significant (P<0.05, Fisher's exact test).

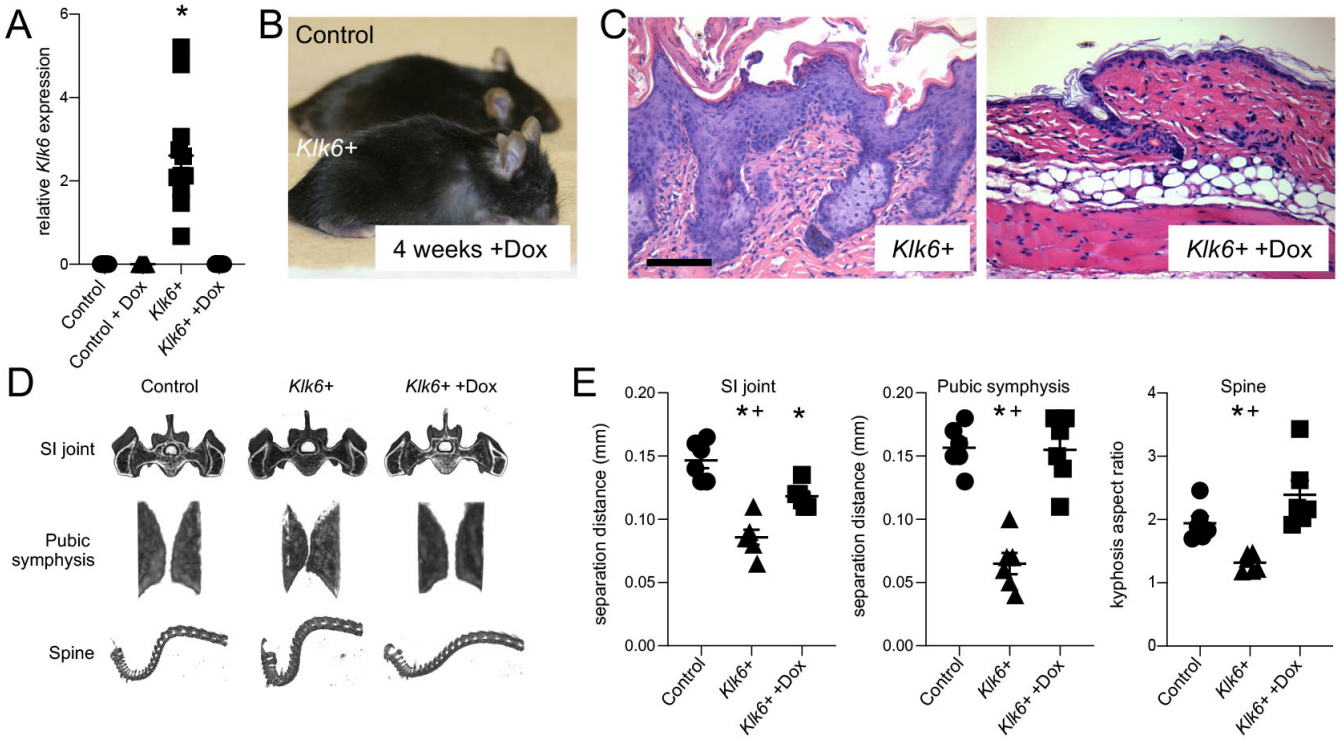

Figure S4. Psoriatic skin and joint abnormalities induced by skin-directed *Klk6* overexpression reverse with normalization of *Klk6* transcript levels.

(A) Detection of *Klk6* mRNA in control and transgenic skin in the absence and presence of doxycycline (Dox) by qRT-PCR. Control +Dox and *Klk6*+ +Dox indicate mice aged to 8-10 weeks to allow for phenotype development in the *Klk6*+ mouse and then transitioned to Dox feed for 4 weeks to repress transgene expression. Transcript levels are normalized to the housekeeping gene *Gapdh*. N=7-11 mice per group. Mean and SEM are indicated. *, P<0.0001 vs +Dox and control by Ordinary one-way ANOVA with post hoc Tukey's multiple comparisons test.

(B) Gross images of control and *Klk6*+ +Dox transgenic mice.

(C) H&E staining of dorsal skin from *Klk6*+ mice in the absence or presence of Dox. Scale bar, 100μm.

(D) Micro-CT images of the sacroiliac (SI) joint, pubic symphysis, and cervico-thoracic kyphosis in control, *Klk6*+, and *Klk6*+ +Dox mice.

(E) Quantitative analysis of micro-CT images of the SI joint, pubic symphysis, and cervico-thoracic kyphosis (spine) in control, *Klk6*+, and *Klk6*+ +Dox mice. Mean and SEM are indicated. N=6 per group. *, P<0.05 vs control; +, P<0.05 vs *Klk6*+ +Dox by Ordinary one-way ANOVA with post hoc Tukey's multiple comparisons test. Control and *Klk6*+ data are reproduced in **Figure 4C**.

Additional supplemental item titles and legends

Video S1. Skin-directed *Klk6* overexpression causes skin erythema and scaling as well as spinal kyphosis and abnormal gait. Mouse was recorded at ~10 weeks of age.

Table S1. Taqman assays used in this study. Primers were purchased from Thermo Fisher Scientific.

Species	Catalog #	Assay ID
Human *IL1B*	4331182	Hs01555410_m1
Human *RPLP0*	4331182	Hs00420895_gH
Human *CXCL1*	4331182	Hs00236937_m1
Human *CXCL2*	4331182	Hs00601975_m1
Human *KLK5*	4331182	Hs01548153_m1
Human *KLK6*	4331182	Hs00160519_m1
Human *KLK8*	4331182	Hs01012737_m1
Human *KLK9*	4331182	Hs01043981_m1
Human *KLK13*	4331182	Hs01087307_m1
Mouse *Gapdh*	4453320	Mm99999915_g1
Mouse *Klk6*	4448892	Mm00478322_m1

Table S2. List of differentially-enriched genes (DEGs) identified in *Klk6*+ transgenic dorsal skin. Coding (sheet 1) and non-coding (sheet 2) DEGs are ranked by fold change (FC) in *Klk6*+ vs WT. FDR, false discovery rate. FPKM, fragments per kilobase of transcript per million mapped reads.

Supplemental Methods

Animals

Klk6 tetracycline responder line: *Tet^{os}-Klk6+* transgenic plasmid DNA was generated as follows: The coding sequence of murine *Klk6* (217-978bp; NM_011177) was PCR amplified and cloned in *pcDNA™3.1-Myc/His version A* linearized with HindIII and XhoI restriction enzymes. The stop codon and preceding codon were then mutated (ctg TGA > ctc gag) to enable expression of a Klk6-Myc/His fusion protein. The fusion transgene was next subcloned using EcoRI and BglII into the *pTet^{OS}* vector (1). Following sequence verification, the *pTet^{OS}-Klk6-Myc/His* transgenic cassette was isolated by SalI restriction enzyme digest, gel purified, and microinjected into C57BL/6 mouse oocytes by the Case Transgenic and Targeting Core of Case Western Reserve University. Transgenic offspring were identified using the following genotyping primers: forward (*Tet^{os}*), ACC ATG TTC ATG CCT TCT T reverse (*Klk6*), CAC TGA GAT TTG CCT TTG G. 10 different founder lines were generated. Each line was mated with C57BL/6 mice to generate F2 offspring.

Generation of binary, keratinocyte-specific, doxycycline repressible, *Klk6* overexpressing mice: F2 *Tet^{os}-Klk6* offspring that were genetically positive for *Tet^{os}-Klk6* were next mated to the keratinocyte-directed tetracycline transactivator (Tet^{off}) driver line *K5-tTA* (2). Dr. Adam Glick (Penn State University, University Park) generously provided the *K5-tTA* line. This line was backcrossed >10 generations to the C57BL/6 background prior to use in these experiments. In the *K5-tTA* line, the bovine *K5* promoter drives expression of the tetracycline transactivator (tTA) primarily in keratinocytes, although expression is detected in some other stratified squamous epithelia; notably, initial characterization of this promoter revealed no expression in small and large bowel (3); consistent with this, we detected no *Klk6* upregulation by qPCR in colon in *Klk6+* transgenic animals (data not shown). We have also confirmed the expression pattern of this promoter in a previous publication by visualizing beta-galactosidase activity in organs harvested from in *K5tTA* x *Tet^{os} nuclear localization signal (nls) LacZ reporter* responder mice (4) . This confirmed robust epidermal

expression and no expression in brain cortex, spleen, lung, heart, kidney, liver, aorta, and aortic root. In the absence of the tetracycline analog doxycycline, tTA binds the tetracycline response element (TRE) upstream of the *Klk6* transgenic coding sequence, activating transgene expression in keratinocytes. In the presence of doxycycline, tTA is bound by doxycycline and rendered incapable of binding the TRE, repressing transgene expression. When crossing *Tet^{os}-Klk6* mice with the *K5-tTA* driver line in the absence of doxycycline, 10 litters yielded no transgenic offspring, indicating that embryonic overexpression of *Klk6* in keratinocytes likely led to embryonic lethality. Mice were then mated in the presence of doxycycline, resulting in successful generation of *Tet^{os}-Klk6* mice carrying the *K5-tTA* driver, hereafter termed *Klk6+* mice for simplicity. For transgene activation and phenotype induction, doxycycline was removed between postnatal days 4 and 7. These mice were characterized for skin *Klk6* expression, ability to generate viable litters, and the development of a reproducible and similar skin phenotype. After extensive characterization and comparison, lines 4 and 5 when mated with *K5-tTA* mice were found to express similar levels of *Klk6* and develop similar skin, joint, and bone phenotypes. *Klk6* mRNA expression in dorsal skin of transgenic mice was an average of 670-fold that of WT (**Figure S1**). Comparing human lesional psoriatic skin to healthy control skin, *KLK6* expression is 5.8-fold higher in psoriasis on average. However, the range of *KLK6* detection is fairly broad: normalizing average expression in healthy control skin to a value of 1, for the raw data depicted in **Figure 1B**, control skin shows a relative range of 0.016-5.00 and lesional psoriatic skin a relative range of 0.92-25.84. Thus, there is a 300-fold range within normal values and a >1600-fold difference between the lowest-expressing healthy control skin and the highest-expressing psoriatic lesional skin. Therefore, while the degree of *Klk6* overexpression in the skin of the transgenic mouse is likely supraphysiologic, given the broad range of tolerance for *KLK6* expression in individuals without psoriasis, it was our intent to highly overexpress *Klk6* to ensure a sufficiently penetrant and informative phenotype that expresses early in the mouse's life.

Klk6+ transgenic and *K5-tTA* driver lines were maintained by backcrossing to C57BL/6 mice, and only transgenic mice from the F4 generation and onward were used for analyses. Littermates inheriting a single, non-expressing transgene (*Tet^{os}-Klk6* or *K5-tTA*) or wild-type littermates served as controls. For transgene repression and phenotype suppression, *Klk6+* mice were maintained as above until reintroduction of doxycycline chow at 10-11 weeks, just prior to cessation of *per os* intake and becoming moribund. Animals were then euthanized and tissues collected and examined at 14-16 weeks of age.

Par1 (B6.129S4-F2r^{tm1Ajc}/J, Stock No 002862) and *Par2* (B6.Cg-F2rl1^{tm1Mslb}/J, Stock No 004993) knockout (KO) mice were ordered from The Jackson Laboratory (Bar Harbor) and crossed to introduce the *Tet^{os}-Klk6* and *K5-tTA* transgenes individually into these KO backgrounds. The resulting single transgenic KO mice were then crossed as described above to generate *Klk6+* KO mice

Tissue collection

Mouse skin was acquired as described previously (5). Mouse tissue was collected from transgenic and control mice following euthanasia.

Fresh human skin samples were acquired by 6mm punch biopsy from psoriasis patients and healthy controls.

To generate RNA, skin samples were then snap-frozen in liquid nitrogen, pulverized, and dissolved in Buffer RLT (Qiagen) for RNA extraction. RNA was isolated using the RNeasy Mini kit (Qiagen).

Quantitative reverse transcription PCR (qRT-PCR)

cDNA synthesis was performed using a High-Capacity cDNA Reverse Transcription Kit (Applied Biosystems Inc.) and qRT-PCR performed with a Prism 7700 Sequence Detector (Applied

Biosystems). TaqMan primer sets and probes were purchased from Applied Biosystems by Life Technologies (**Table S1**). All values were normalized to the expression of housekeeping genes (*RPLP0*, human; *Gapdh*, mouse). qRT-PCR data in **Figure 1B** are presented with whisker plots. In these graphs, the box extends from 25th-75th percentile, the mean is indicated, and whiskers depict minimum and maximum values. qRT-PCR data in **Supplemental Figure 4A** are presented with a scatter plot with the mean and SEM indicated. P values were determined using an Ordinary one-way ANOVA with post hoc Tukey's multiple comparisons test. $P<0.05$ was considered statistically significant.

Cell culture

Vorapaxar was obtained from Axon Medchem (1755) and dissolved in dimethyl sulfoxide at a concentration of 10mM to generate soluble vorapaxar. Skin explants were isolated from psoriasis patients as follows: 4 6mm punch biopsies from lesional psoriatic skin were obtained from 4 psoriasis patients. Biopsies were quartered. Each quarter was placed in a 48 well plate with 500ul of Iscove's Modified Dulbecco's Medium with 1% human AB serum (Lonza (Cambrex Bio Science) Walkersville, Inc., 14-490E) and penicillin/streptomycin/amphotericin B. Tissue was cultured in the presence or absence of soluble vorapaxar at 100nM concentration for 24 hours. Supernatants and tissue were harvested for RNA isolation and analyzed as above.

Histology and immunostaining

Hematoxylin (Surgipath, 3801540) & eosin (Surgipath, 3801600) (H&E) staining was performed per standard protocols.

Immunohistochemistry was performed on fresh frozen tissue sections as previously described (6) using the following antibodies: goat anti-human KLK6 (R&D Systems, #AF2008, lot #KJB01), rabbit anti-human PAR1 (LifeSpan BioSciences, Inc., LS-C405766), rat anti-mouse CD4 (BD Biosciences,

550280), rat anti-mouse CD8a (BD Biosciences, 550281), rat anti-mouse GR1 (BD Biosciences, 550-291), hamster anti-mouse CD11c (BD Biosciences, 550283), rat anti-mouse F4/80 (eBioscience, 14-4801-82), rat anti-mouse MECA-32 (Developmental Studies Hybridoma Bank, MECA-32-s), rat anti-mouse Ki-67 (DAKO, M7249), and rabbit anti-phospho-Stat3 (Tyr705) (D3A7) XP (Cell Signaling Technology 9145). Antibodies were detected using either rabbit anti-rat IgG biotinylated, goat anti-rabbit IgG biotinylated (Vector Laboratories), or rabbit anti-hamster IgG biotinylated (Southern Biotech) secondary antibodies, amplified with Avidin/Biotinylated Enzyme Complex (Vector), and visualized using the enzyme substrate diaminobenzidine (Vector). Slides were counterstained with hematoxylin. Images were captured using a Leica DM L82 microscope with an attached QImaging MicroPublisher 3.3 camera and Q-capture Pro software (QImaging).

Immunofluorescence was performed as follows: Formalin fixed, paraffin-embedded tissue sections were deparaffinized, rehydrated, and heated at 95°C for 20 min in pH 6 antigen retrieval buffer. Slides were blocked and incubated with PAR1 (LifeSpan BioSciences, Inc., LS-C405766) and CD3 (Abcam, ab17143) antibodies overnight at 4°C, incubated with Alexa Fluor 488 AffiniPure Donkey Anti-Mouse (Jackson ImmunoResearch Labs, 715-545-151) and Alexa Fluor 594 AffiniPure Donkey Anti-Rabbit (Jackson ImmunoResearch Labs, 711-585-152) as appropriate, and mounted. Images were acquired using Zeiss Axioskop 2 microscope and analyzed by SPOT software V.5.1.

Histopathological assessment of the joints was performed on paraffin-embedded H&E-stained sections by a blinded investigator. Enthesitis was evaluated based on three parameters: inflammatory infiltrate in the tendon, inflammation of the synovial tissue, and bone erosion. Histopathological assessment of the spines was performed on paraffin-embedded H&E stained sections by author RM, an investigator with bone expertise.

Micro-computed tomography (micro-CT) imaging and bone morphometric analysis

Whole mice (N≥5 for each group) were scanned on a GE Locus RS in-vivo micro-CT equipped with a rotating gantry. Images were obtained using an X-ray tube voltage of 80 kV and a tube current of 450 μA with exposure time of 400 ms. Using a 1º angle of increment, 360 raw data projections were acquired. Then, 2 frames per degree were averaged for a resultant image that was later utilized for reconstruction. Reconstruction of images was performed by GE algorithms using a 16-core cluster UNIX PC. For whole mouse scans, the detector binning was set to achieve an isotropic voxel resolution of 45 μm. Sacro-iliac and pubic joint spaces were evaluated at a higher resolution of 20 μm.

Bone structure and mineral density metrics from the T11 vertebral body were evaluated using GE Microview software. Post-acquisition reconstructed micro-CT volumes were calibrated using air, a solid water phantom, and a cortical bone phantom. The micro-CT volume grayscale values (correlated to Hounsfield units) were normalized to the phantom so that a standard grayscale threshold level could be applied to all vertebral body volumes for bone metrics. Regions of interest were manually selected using software splining tools for subsequent analysis and generation of global threshold-based metrics.

Animals were evaluated for the presence of kyphosis by registering their volumes in space and taking point-to-point measurements in the anterior-posterior and dorsal-ventral aspects. An example of a spine image (WT, adjacent image) provides a diagram of the measurements of micro-CT spine images used to assess spine curvature. Briefly, the length (L) of the spine curvature was

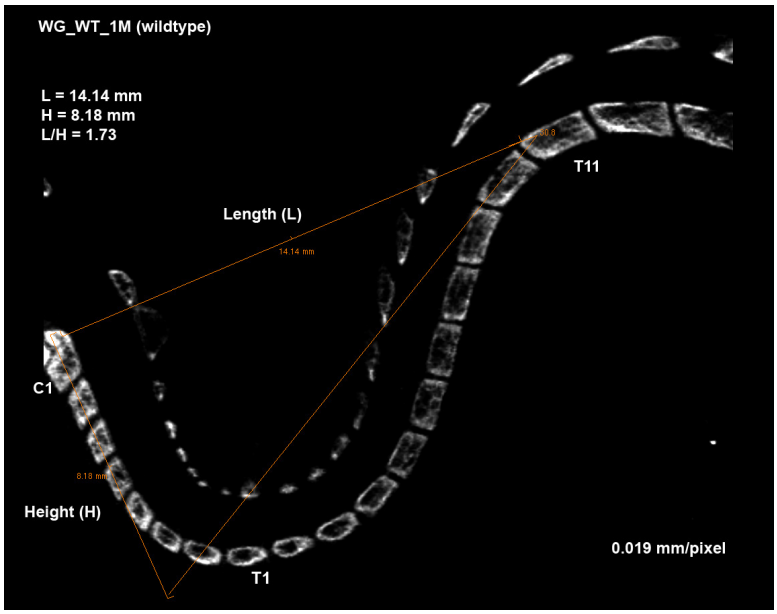

measured from C1 to T11 vertebrae and the height (H) of the spine curvature was measured from C1 to T1 vertebrae (see adjacent image). The L/H ratio value for each sample was used to determine the measure of spine curvature for each mouse.

The pubic symphysis joint space was evaluated for separation distance and/or fusion. Volumes were registered in space, and 5 point-to-point measurements were taken across the joint space and averaged into a single value. The same approach was applied to the sacro-iliac joint space; however, 5 measurements were taken for each side of the animal, then averaged, respectively.

Enzyme-linked immunosorbent assay (ELISA)

ELISA was performed on mouse skin as previously described (5). Murine IL-17A (R&D Biosystems, M1700), IL-12/23p40 subunit (R&D Biosystems, MP400), IL-23p19 subunit (R&D Biosystems, M2300), and IL-6 (R&D Biosystems, M6000B) protein levels were quantitated using ELISA according to the manufacturer's instructions.

Human *KLK* gene expression analysis

Analysis of *KLK* transcript levels presented was performed as follows: RNA-seq data from punch biopsies isolated from lesional skin of 99 psoriasis patients, non-lesional skin of 27 psoriasis patients, and normal skin of 90 healthy controls (GSE63980) were analyzed using the pipeline and gene models described previously for RNA-seq analysis, including read mapping, assembly, and gene expression quantification (7). Rank-based inverse normalization was then applied to each gene's normalized expression values for plotting. P values were computed using Wilcoxon rank-sum test (8), and false discovery rate (FDR) was used to control the multiple testing.

Gene expression analysis during etanercept therapy

Analysis of *KLK6* and *S100A7/psoriasin* transcript levels during etanercept therapy: RNA-seq data were analyzed from 14 psoriasis patients who received etanercept therapy. Following treatment, 14 patients achieved a 75% reduction in the Psoriasis Area and Severity Index (PASI) score (PASI 75), a common primary endpoint for psoriasis therapy clinical trials, and were classified as drug responders. Samples corresponded to skin biopsies isolated from non-lesional skin taken at time 0 and from lesional skin taken at 0, 2, 6, and 12 weeks of therapy. **Figure 1D** illustrates the expression level of genes measured by the RNA-seq in the 14 drug responders. Box and whisker plots were generated using normalized expression values and P values computed using negative binomial test (9). The read count in the RNA-seq data was modeled using negative binomial to capture the over dispersion of the data, and then generalized linear model was used to conduct differential expression analysis (i.e., PN w0 vs PP w0; or PP w0 vs PP w2/6/12). Whiskers were defined as follows: The top whisker has the range between the 75th percentile of the expression values to the value of: 75th percentile + 1.5 x (75th percentile - 25th percentile), while the bottom whisker is between 25th percentile to the value of: 25th percentile - 1.5 x (75th percentile - 25th percentile).

RNA-sequencing (RNA-seq) protocol

Murine samples were submitted to a core facility for sequencing (University of Michigan, Ann Arbor, MI). Sample preparation was performed using the Illumina TruSeq mRNA Sample Prep v2 kit (catalog no. RS-122-2001 and RS-122-2002). Preparation of mRNA via polyA purification was carried out using 0.1–3.0 μg of total RNA per sample. mRNA was converted to cDNA using reverse transcriptase and random primers, and cDNA libraries were enriched and purified using Kapa's library quantification kit (catalog no. KK4835; Kapa Biosystems, Wilmington, MA, USA). cDNA quantification and quality assessment was performed using the Agilent TapeStation. The Illumina clonal amplification system (cBot) was used to cluster samples with adaptor barcodes prior to Illumina HiSeq 2000 sequencing (50-cycle single end).

Reference-based read alignment

FastQC was used to perform initial quality assessments of fastq sequence files (10). Adaptor sequences (AGATCGGAAGAGC) were removed using Cutadapt with a maximum error rate of 5% (-e 0.05) (11). Cudadapt was then used to quality filter reads using asci (phred quality + 33) threshold of 30 (-q 30) and minimum read length of 20 (--minimum-length 20). A window-based filter was also applied using the FASTX-Toolkit program “fastq_quality_filter” (12), which required reads to have quality scores above 30 for at least 50% of the read length. There remained an average of 41.5 million reads per sample following these filtering steps.

Quality-filtered reads were mapped to the UCSC GRCm38/mm10 genome using Tophat2 (13). Default settings were applied with disabling of multi-mapping (-g 1) and the coverage-based search for junctions (--no-coverage-search). This generated an aligment bam file for each sample that was subsequently sorted and indexed using samtools (14). The number of reads aligned to each genomic feature was tabulated using the HTSeq library and “htseq-count” algorithm (15). A read was required to completely overlap the reference gene’s sequence to be tabulated as a mapped read (-m intersection-strict). FPKM and associated confidence intervals were calculated using Cufflinks (version 2.2.1) with default settings (16). RSeQC (17) and RNA-SeQC (18) were used to assess the quality of sequencing alignments.

Among the 10 samples, an average of 97.4% of quality-filtered reads were successfully aligned to the mm10 genome, with an intragenic mapping rate of 92% and exonic mapping rate of 89.2%. Only 3.3% of reads on average aligned to ribosomal RNA sequences. For each sample, a gene was considered to have detectable expression if at least 1 read was mapped to its sequence and if the FPKM lower 95% confidence limit was greater than 0. Based on these criteria, an average of 15365 protein-coding genes per sample had detectable expression (range: 15053-15624).

Differential expression analysis

Differential expression analysis was performed to identify genes with altered expression in skin from *Klk6*+ transgenic mice (N=3 males, 2 females) as compared to WT mice (N=3 males, 2 females). Differentially expressed genes (DEGs) were identified using the negative binomial modeling approach implemented in edgeR (19). Normalization factors applied to each sample were calculated using the weighted trimmed mean of M values method (20). Empirical Bayes dispersion parameters were calculated for each feature (edgeR function: estimateGLMTagwiseDisp)(21). Negative binomial generalized log-linear models were then fit using the "glmFit" function with both sex (male vs female) and treatment (*Klk6*+ vs WT) as covariates. The significance of treatment effects for each gene feature was evaluated using likelihood ratio tests (edgeR function: glmLRT), which compared goodness of fit between full models (sex + treatment) and reduced models lacking the treatment effect covariate. Raw P values generated from differential expression tests were adjusted to control the false discovery rate (FDR) using the Benjamini-Hochberg correction (22). DEGs were identified as those genes with expression increased or decreased more than 2-fold with FDR < 0.10.

DEG characterization and human psoriasis comparisons

Conditional hypergeometric tests were used to determine if specific gene annotation terms were disproportionately associated with DEGs we identified (R package: GOstats) (23). Analyses were carried out with respect to Gene Ontology (GO) biological process (BP) terms (24) and the Kyoto Encyclopedia of Genes and Genomes (KEGG) database (25) (**Figure S1**).

Gene expression changes in the *Klk6*+ vs WT comparison were compared to changes observed in lesions from human psoriasis patients (**Figure 2F**). Analyses were performed using matched mouse-human orthologue gene pairs. First, we compared mouse differential expression patterns to those observed in lesional skin from psoriasis patients (PP) vs non-lesional skin from psoriasis patients (PN). PP vs PN differential expression results were obtained from a prior meta-analysis of three

studies (GSE41745, GSE54456/GSE63979, GSE66511) including an aggregate total of samples from 44 patients (26). Second, we compared mouse differential expression patterns to those observed in lesional skin from psoriasis patients with psoriatic arthritis (PP-PsA) vs lesional skin from psoriasis patients with cutaneous-only psoriasis (PP-PsC).

For the PP-PsA vs PP-PsC comparison, lesional skin samples were evaluated from GEO datasets GSE54456 and GSE63979 (7, 8). Comparisons included lesional skin samples from 67 PP-PsC patients and 18 PP-PsA patients (GSM1315623, GSM1315627, GSM1315629, GSM1315631, GSM1315634, GSM1315640, GSM1315687, GSM1315690, GSM1315693, GSM1315702, GSM1315703, GSM1315740, GSM1315752, GSM1315769, GSM1315775, GSM1315776, GSM1315777, GSM1561641). Differential expression between PP-PsA and PP-PsC samples was performed using the negative binomial modeling approach described above (R package: edgeR) (19). Patient sex was included as a covariate in full and reduced models, with likelihood ratio tests used to compare goodness of fit between models with and without the covariate specifying disease status (PsA vs PsC).

The Spearman rank correlation was used to assess mouse-human correspondence of FC estimates, and overlap between increased and decreased DEG sets was assessed using Fisher's exact test (27). Enrichment of PsA-increased and PsA-decreased DEGs relative to the list of genes ranked according to their expression change in *Klk6*+ vs WT mice was evaluated using detection rate curve gene set enrichment analysis (28). The overlap between ordered lists of top-ranked genes was assessed by comparison observed overlap to that expected given a hypergeometric null distribution (29).

Supplemental references

1. Sarao R, and Dumont DJ. Conditional transgene expression in endothelial cells. *Transgenic Res.* 1998;7(6):421-7.
2. Diamond I, Owolabi T, Marco M, Lam C, and Glick A. Conditional gene expression in the epidermis of transgenic mice using the tetracycline-regulated transactivators tTA and rTA linked to the keratin 5 promoter. *J Invest Dermatol.* 2000;115(5):788-94.
3. Ramirez A, Bravo A, Jorcano JL, and Vidal M. Sequences 5' of the bovine keratin 5 gene direct tissue- and cell-type-specific expression of a lacZ gene in the adult and during development. *Differentiation.* 1994;58(1):53-64.
4. Wang Y, Gao H, Loyd CM, Fu W, Diaconu D, Liu S, et al. Chronic skin-specific inflammation promotes vascular inflammation and thrombosis. *J Invest Dermatol.* 2012;132(8):2067-75.
5. Wolfram JA, Diaconu D, Hatala DA, Rastegar J, Knutsen DA, Lowther A, et al. Keratinocyte but not endothelial cell-specific overexpression of Tie2 leads to the development of psoriasis. *Am J Pathol.* 2009;174(4):1443-58.
6. Johnston A, Fritz Y, Dawes SM, Diaconu D, Al-Attar PM, Guzman AM, et al. Keratinocyte overexpression of IL-17C promotes psoriasiform skin inflammation. *J Immunol.* 2013;190(5):2252-62.
7. Tsoi LC, Iyer MK, Stuart PE, Swindell WR, Gudjonsson JE, Tejasvi T, et al. Analysis of long non-coding RNAs highlights tissue-specific expression patterns and epigenetic profiles in normal and psoriatic skin. *Genome Biol.* 2015;16:24.
8. Li B, Tsoi LC, Swindell WR, Gudjonsson JE, Tejasvi T, Johnston A, et al. Transcriptome analysis of psoriasis in a large case-control sample: RNA-seq provides insights into disease mechanisms. *J Invest Dermatol.* 2014;134(7):1828-38.
9. Love MI, Huber W, and Anders S. Moderated estimation of fold change and dispersion for RNA-seq data with DESeq2. *Genome Biol.* 2014;15(12):550.

10. Andrews S. FastQC: A quality control tool for high throughput sequence data. http://www.bioinformatics.babraham.ac.uk/projects/fastqc/. Accessed February 15, 2015.
11. Martin M. Cutadapt removes adapter sequences from high-throughput sequencing reads. *EMBnetjournal.* 2011;17:10-2.
12. Hannon GJ. FASTX-Toolkit. http://hannonlab.cshl.edu/fastx_toolkit/
13. Kim D, Pertea G, Trapnell C, Pimentel H, Kelley R, and Salzberg SL. TopHat2: accurate alignment of transcriptomes in the presence of insertions, deletions and gene fusions. *Genome Biol.* 2013;14(4):R36.
14. Li H, Handsaker B, Wysoker A, Fennell T, Ruan J, Homer N, et al. The Sequence Alignment/Map format and SAMtools. *Bioinformatics.* 2009;25(16):2078-9.
15. Anders S, Pyl PT, and Huber W. HTSeq-a Python framework to work with high-throughput sequencing data. *Bioinformatics.* 2015;31(2):166-9.
16. Trapnell C, Roberts A, Goff L, Pertea G, Kim D, Kelley DR, et al. Differential gene and transcript expression analysis of RNA-seq experiments with TopHat and Cufflinks. *Nat Protoc.* 2012;7(3):562-78.
17. Wang L, Wang S, and Li W. RSeQC: quality control of RNA-seq experiments. *Bioinformatics.* 2012;28(16):2184-5.
18. DeLuca DS, Levin JZ, Sivachenko A, Fennell T, Nazaire MD, Williams C, et al. RNA-SeQC: RNA-seq metrics for quality control and process optimization. *Bioinformatics.* 2012;28(11):1530-2.
19. Robinson MD, McCarthy DJ, and Smyth GK. edgeR: a Bioconductor package for differential expression analysis of digital gene expression data. *Bioinformatics.* 2010;26(1):139-40.
20. Robinson MD, and Oshlack A. A scaling normalization method for differential expression analysis of RNA-seq data. *Genome Biol.* 2010;11(3):R25.
21. Landau WM, and Liu P. Dispersion estimation and its effect on test performance in RNA-seq data analysis: a simulation-based comparison of methods. *PloS one.* 2013;8(12):e81415.

22. Benjamini Y, and Hochberg Y. Controlling the false discovery rate: a powerful and practical approach to multiple testing. *J Roy Stat Soc B.* 1995;57:289–300.

23. Falcon S, and Gentleman R. Using GOstats to test gene lists for GO term association. *Bioinformatics.* 2007;23(2):257-8.

24. Blake JA, Dolan M, Drabkin H, Hill DP, Li N, Sitnikov D, et al. Gene Ontology annotations and resources. *Nucleic Acids Res.* 2013;41(Database issue):D530-5.

25. Kanehisa M, Sato Y, Kawashima M, Furumichi M, and Tanabe M. KEGG as a reference resource for gene and protein annotation. *Nucleic Acids Res.* 2016;44(D1):D457-62.

26. Swindell WR, Sarkar MK, Liang Y, Xing X, and Gudjonsson JE. Cross-Disease Transcriptomics: Unique IL-17A Signaling in Psoriasis Lesions and an Autoimmune PBMC Signature. *J Invest Dermatol.* 2016.

27. Sokal RR. *Biometry; the principles and practice of statistics in biological research.* San Francisco: W. H. Freeman; 1969.

28. Philippakis AA, Busser BW, Gisselbrecht SS, He FS, Estrada B, Michelson AM, et al. Expression-guided in silico evaluation of candidate cis regulatory codes for Drosophila muscle founder cells. *PLoS Comput Biol.* 2006;2(5):e53.

29. Lottaz C, Yang X, Scheid S, and Spang R. OrderedList--a bioconductor package for detecting similarity in ordered gene lists. *Bioinformatics.* 2006;22(18):2315-6.